Tunable Sensitivity in Long Period Fiber Gratings During Mode Transition With Low Refractive Index Intermediate Layer

Ignacio Del Villar, Jorge Montoya-Cardona, José J. Imas, Erick Reyes-Vera, Carlos R. Zamarreño, Ignacio R. Matias, and Jose L. Cruz

***Abstract*—Double-clad fibers where the second cladding has a lower refractive index than the first cladding, prove to be ideal structures for potentiating and tuning the sensitivity in long-period fiber gratings (LPFGs) operating in mode transition. When a thin film is deposited on the optical fiber, the second cladding performs acts as a barrier that initially prevents the transition to guidance in the thin film of one of the modes guided in the first cladding. Finally, the transition to guidance occurs with a sensitivity increase, in analogy to the tunnel effect observed in semiconductors. This improvement has been demonstrated both as a function of the thin film thickness and the surrounding medium refractive index, with enhancement factors of 4 and 2, respectively. This idea reinforces the performance of LPFGs, adding a new degree of freedom to the mode transition and the dispersion turning point phenomena. Moreover, the control of the variation of the effective index of cladding modes could be applied in other structures, such as tilted-fiber gratings or evanescent wave sensors.**

***Index Terms*—Etching, long period fiber grating (LPFG), mode transition, sensors, thin film, tunnel effect.**

I. Introduction

Lomg-period fiber gratings (LPFGs) permit to generate resonance notches in the transmission spectrum by coupling the core mode to copropagating cladding modes, and they were experimentally demonstrated with the aid of UV photoin- scription [1], [2]. Soon afterwards, the capability of sensing different parameters, such as temperature, strain and refractive index was demonstrated; even dual sensors were developed [3]. LPFGs are wavelength based optical fiber sensors [4]. This means that the detection of a specific parameter is based on the wavelength shift of the resonance notches. According to this, the sensitivity of each resonance of the LPFG is the ratio between the wavelength shift of the resonance and the variation of the pa- rameter to detect, being the surrounding medium refractive index the most extended parameter for assessing the performance of the optical structure [5].

Up to now, three major achievements have boosted the per- formance of LPFGs. The first is the dispersion turning point [6], which is characterized by the generation of dual resonance bands induced by the same cladding mode and results in very high sensitivity. This is typically achieved with high-order cladding modes, though with an appropriate design, dual resonances can be observed with low-order modes [7]. The second major phe- nomenon that potentiates the performance of LPFGs is related to the deposition of a thin film onto its cladding. The progres- sive deposition of nanometric thin films produces a wavelength shift in the resonance bands whose point of highest sensitivity matches the transition to guidance of a cladding mode in the thin film [8], [9]. This phenomenon is known as mode transition [10], and can be combined with the dispersion turning point to obtain very high sensitivities [11], [12].

Moreover, the reduction in the cladding diameter of the LPFG, typically by an etching process, also increases the sensitivity of the device [13]. Thus, cladding diameter reduction is the third way to improve the performance of an LPFG. The latter can be combined with the other two techniques to achieve sensitivities of around 40.000 nm/RIU in the water region [14], which results in LPFGs being among the best optical fiber sensors in terms of sensitivity [15]

Here we propose a fourth way to improve the sensitivity of LPFGs, on the basis of a theoretical work published in 2006 [16]. In that work, it was proposed to include a low-RI layer acting as a second cladding between the thin film and the cladding of the LPFG. This layer operates as a barrier for the guidance of the cladding mode in the high-RI thin film, in analogy to the tunnel effect observed in electronics. Finally, the cladding mode can be guided in the thin film by tunneling the narrow thickness of the low-RI region, producing a mode transition. The rate of change of the wavelength shifts of the resonances during the mode transition can be controlled through the thickness of the low-RI region.

It might be surprising that experimental evidence of this phenomenon has not yet been demonstrated by the scientific community, but it must be pointed out that the experiment is extremely challenging. The resonance bands in the mode transition fade very easily when an absorptive material is deposited with techniques such as Langmuir–Blodgett or layer-by-layer (LbL) self-assembly [17], [18]. Dip-coating was the first alternative to solve this issue and attain good results during the full mode transition regions [19], though more sophisticated techniques such as atomic layer deposition (ALD) can be applied for the same purpose [20].

It must be mentioned that the mode transition has been demonstrated in double-clad fibers [21], [22], although the configuration is completely different from the one proposed in the previous paragraph. In these publications the grating was inscribed in a fiber W-type RI profile, that is, the refractive index of the second cladding is higher than that of the first cladding; and no thin film is deposited. Therefore, the number of layers and the RI profile is the same as in the case of the standard LPFG deposited with a high RI thin film, with the only difference that the mode transition is achieved by etching the second cladding instead of by depositing a thin film.

Here, we propose for the first time an experimental study about the mode transition obtained through the deposition of a high RI thin film on a double-clad fiber where the refractive index of the second cladding is lower than that of the first cladding (see Fig. 1(a)). In the first place, fibers with different second cladding thicknesses will be obtained by means of etching. The final thickness will be controlled through the wavelength shift during the etching process. Then, the mode transition obtained through the deposition of a high RI thin film will be studied for these fibers, assessing the impact of the second cladding thickness on the sensitivity to the thin film thickness. Finally, the sensitivity to the surrounding medium refractive index (SRI) will be analyzed for fibers working at the mode transition with different second cladding thicknesses.

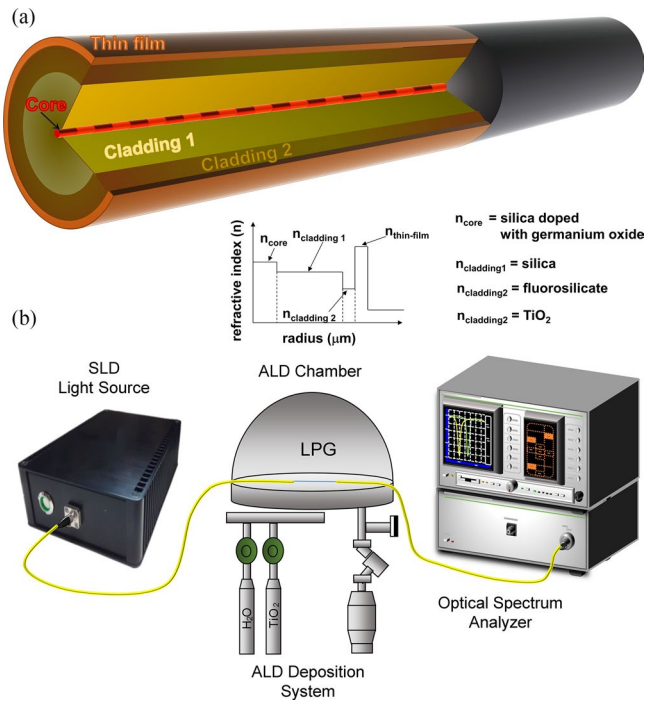

Fig. 1. Optical fiber structure and deposition process. (a) Four-layer structure with core, two claddings and a thin film. (b) Each LPFG is introduced in the ALD deposition system with the aid of two feedthroughs for monitoring the light received by an optical spectrum analyzer during the deposition.

II. Materials and Methods

A. Long-Period Fiber Grating Fabrication

Gratings with period 176 μm and length 12.5 mm were written in a hydrogen-loaded double-clad fiber SMM900 (105/125) from Fibrecore. The characteristics of the fiber batch used for the experiments were the following. The first and second-cladding diameter were 102 and 124.7 μm, respectively (this leads to a thickness of the second clad of around 11 μm and there is not a need for a deep etching that compromises the uniform thickness of the second clad around de fiber after the etching process). The numerical aperture of the first and second cladding were

0.18 and 0.24, respectively, and the cut-off wavelength 895 nm; this fiber permits single-mode guidance from 915 to more than 1550 nm and becomes very versatile for selecting the appropriate cladding mode order and the operation wavelength (including the telecommunications wavelength range). Finally, the modal field diameter of the core mode was 7.8 μm. The gratings were photo-inscribed point by point with a doubled argon laser, generating a quasi-square-wave profile with a 50% duty cycle. The fibers were stored for 240 hours to allow the out-diffusion of the remaining hydrogen and hence the grating stabilization. Six samples with these characteristics were manufactured for the analysis shown in the results section. Four samples were used for the analysis of sensitivity to nanocoating thickness, with a surrounding RI = 1 (air), and two were used for the analysis of the sensitivity to RI. Fig. 1(a) shows a schematic representation of the cross-section of the four-layer structure composed of core, two claddings and a thin film

B. Etching and Deposition Process

A 30-mm-long segment including the photo-inscribed part of the LPFG was introduced into a plastic cuvette [23]. The cuvette was filled with 25% (v/v) hydrofluoric acid (HF) solution from Panreac, Barcelona, Spain. This concentration permitted a slow and uniform etching process at a rate of 0.7 μm/min in the region of interest.

Regarding the deposition, the atomic layer deposition (ALD) technique was used (Savannah G2 ALD System, Veeco Inc.) employing tetrakis(dimethylamido) titanium(IV) (669008, Sigma-Aldrich) and ultrapure H_20 as precursors. The samples were introduced into the chamber and monitored with the aid of two feedthroughs that permitted connecting the two ends of the fibers to an optical spectrum analyzer (Anritsu MS9030A-MS9701B) and a multi-SLED light source (FJORD-X3-1330-1650, Pyroistech S.L.) during the deposition process (see Fig. 1(b)). The deposition was performed at a constant temperature of 100 °C.

C. Refractive Index Sensing

The two LPFGs designed for the RI sensitivity analysis were immersed in glycerol solutions ranging from RI 1.33–1.47. The RI of the solutions was characterized with a commercial refractometer (Mettler Toledo Refracto 30GS) operating at a wavelength of 589 nm with a precision of 0.001.

D. Simulations

The modal fields and the effective indices of the modes in each section of the LPFG were calculated by the finite difference method (FDM) of FIMMWAVE (Photon Design Inc.), as this is the most accurate method for a cylindrical waveguide. On this basis, the transmission spectra were calculated with FIMMPROP, a module integrated within FIMMWAVE. For the input and output sections of the fiber, only the core mode was simulated, whereas in the grating region both the core mode and up to 14 other modes were calculated in order to include the highest-order mode responsible for the resonances observed in the transmission spectra. Each period consisted of two segments of different RI, implementing in this way a square-wave profile, which resembled the experimental one.

Only the core radius and the dispersion of the core numerical aperture (NA) were used as fitting parameters. NA was in the range 0.176–0.184 in the wavelength range 1200–1700 nm in order to fit the resonances. Regarding the core diameter, the value that best fitted the experimental results was 5 μm. In addition, the peak-to-peak refractive index modulation in the grating region, which is closely related to the depth of the resonances, was set to 0.001 for a best fitting in Fig. 2 between the experimental and the numerical spectrum for one of the LPFGs. Three different bands are observed, which from short to long wavelengths correspond to coupling of the core mode to cladding modes $HE_{1,10}$, $HE_{1,12}$ and $HE_{1,14}$. For the sake of clarity, the notation for the modes is the following: $HE_{1,1}$ for the core mode; $HE_{1,2}$ for the first $HE_{1,x}$ cladding mode, $HE_{1,4}$ for the second $HE_{1,x}$ cladding mode, and so on; and $EH_{1,3}$ for the first $EH_{1,x}$ cladding mode, $EH_{1,5}$ for the second $EH_{1,x}$ cladding mode, and so on.

Henceforward, the experiments will be mainly focused on the band located at a longer wavelength, corresponding to the cladding mode $HE_{1,14}$, because it shows the highest sensitivity (coupling to higher order modes in LPFGs leads to higher sensitivity [24]).

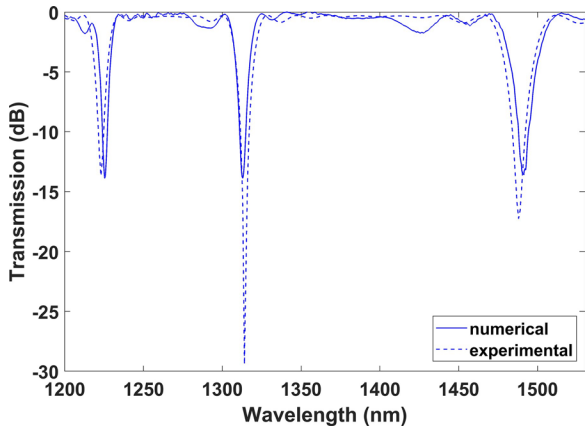

Fig. 2 Numerical and experimental initial transmission spectrum. for an LPFG of period 176 μm in the pristine fiber.

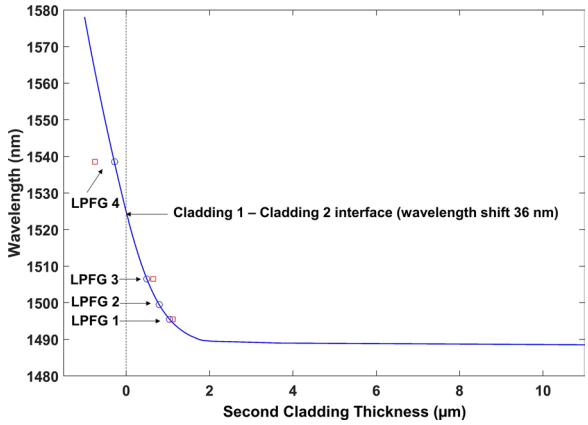

Fig. 3. Wavelength shift of the $HE_{1,14}$ band as a function of second-cladding thickness. The blue circles indicate the theoretical thickness corresponding to the wavelength shift observed in the four etched LPFGs. The red squares show the thickness observed by the microscope for three of these LPFGs.

III. Results and Discussion

A. Control of Second-Cladding Thickness by Etching

In order to verify the hypothesis that the thickness of the second cladding controls the further sensitivity of the device in the mode transition region, four LPFGs with the same characteristics were manufactured and each of them subjected to an etching process. Different thicknesses of the second cladding were obtained as a function of the etching time.

According to this, Fig. 3 shows the simulated wavelength shift of the $HE_{1,14}$ resonance band as function of the second cladding thickness. The x-axis covers up to 11.35 μm, which is the initial thickness of the second cladding before etching.

LPFGs 1, 2, 3 and 4 experienced a wavelength shift of 7, 11, 18 and 50 nm, respectively, as a result of the etching process. Related to this, Fig. 3 shows the theoretical wavelength shift as function of the second clad thickness, where the blue points are the second clad thicknesses corresponding to the experimental wavelength shifts of LPFG 1, 2, 3 and 4: 1.06, 0.79, 048 and −0.28 μm (the negative value means that the second clad hasbeen completely removed and 0.28 μm of the first cladding have been etched). These results correspond with external diameter values of the fiber: 104.12, 103.58, 102.96 and 101.44 μm.

Fig. 4 shows microscope images (obtained with a Leica DM2500M microscope equipped with a Leica DMC2900 camera, both from Leica Microsystems), for three of the LPFGs. Three measurements were made in each sample, with average values of 104.3, 103.3, and 100.5 μm for LPFGs 1, 3, and 4, respectively. These values are represented in Fig. 3 as red points and are quite similar to the theoretical values indicated above. There is no experimental value for LPFG 2 because this fiber was re-etched and reused.

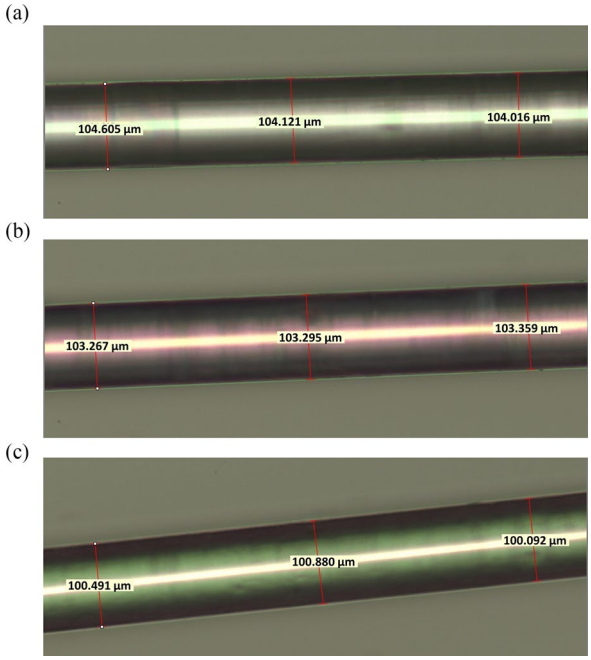

Fig. 4. Microscope images for different thicknesses of cladding 2 after the etching process. They correspond to LPFGs 1, 3 and 4; the etching wavelength shifts during the etching process are 7, 18 and 50 nm, respectively.

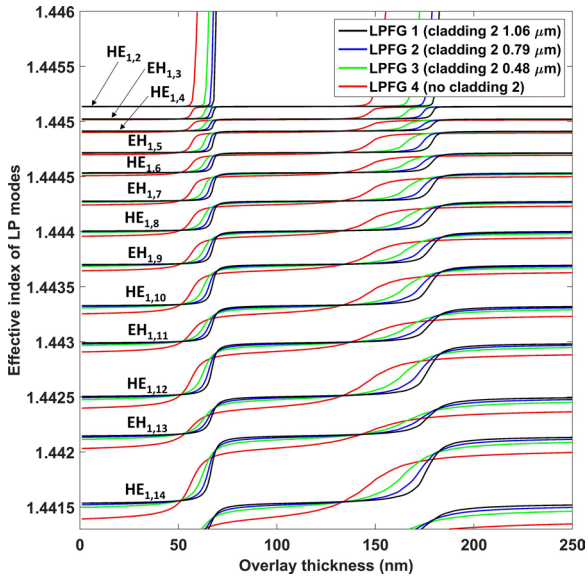

Fig. 5. Effective indices of $HE_{1,x}$ and $EH_{1,x}$ modes as a function of the TiO_2 thin-film thickness.

B. Atomic Layer Deposition and Sensitivity to Thickness

In Fig. 5 the effective indices of the cladding modes are analyzed theoretically at a wavelength of 1450 nm as a function of the thickness of a TiO_2 nanocoating, for the LPFGs obtained in the previous section. The wavelength 1450 nm was selected because it is located in the middle of the mode transition of the resonance that corresponds to mode $HE_{1,14}$, which is the main band analyzed henceforward. The model for TiO_2, obtained with an UVISEL 2 ellipsometer from Horiba, is shown in Fig. 6(a) (the ellipsometer model was based on two depositions of 75 and 216 nm, i.e., the thickness of the first mode transition and the thickness that corresponds with the range analyzed in the paper). Fig. 6(b) shows an SEM photograph of the thin film deposited on LPFG 1 after the etching process. The coating is thicker than the thickness range analyzed throughout the article, 0 to 250 nm, in order to make sure the two step transition was monitored during the deposition. After that, the range from 0 to 250 nm was selected because it permits to observe the two step mode transition with a good perception of the change of the slope depending on the second clad thickness.

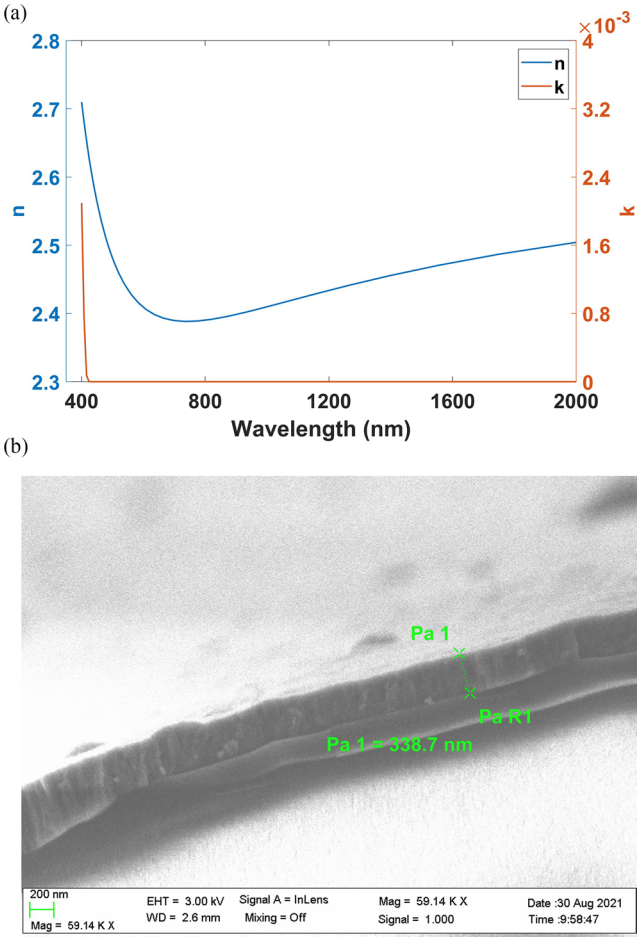

Fig. 6. Thin film characterization: (a) Refractive index (n) and extinction coefficient (k) of TiO_2 as a function of wavelength by ellipsometry. (b) FESEM image of the cross-section of the TiO_2 thin film deposited on LPFG 1.

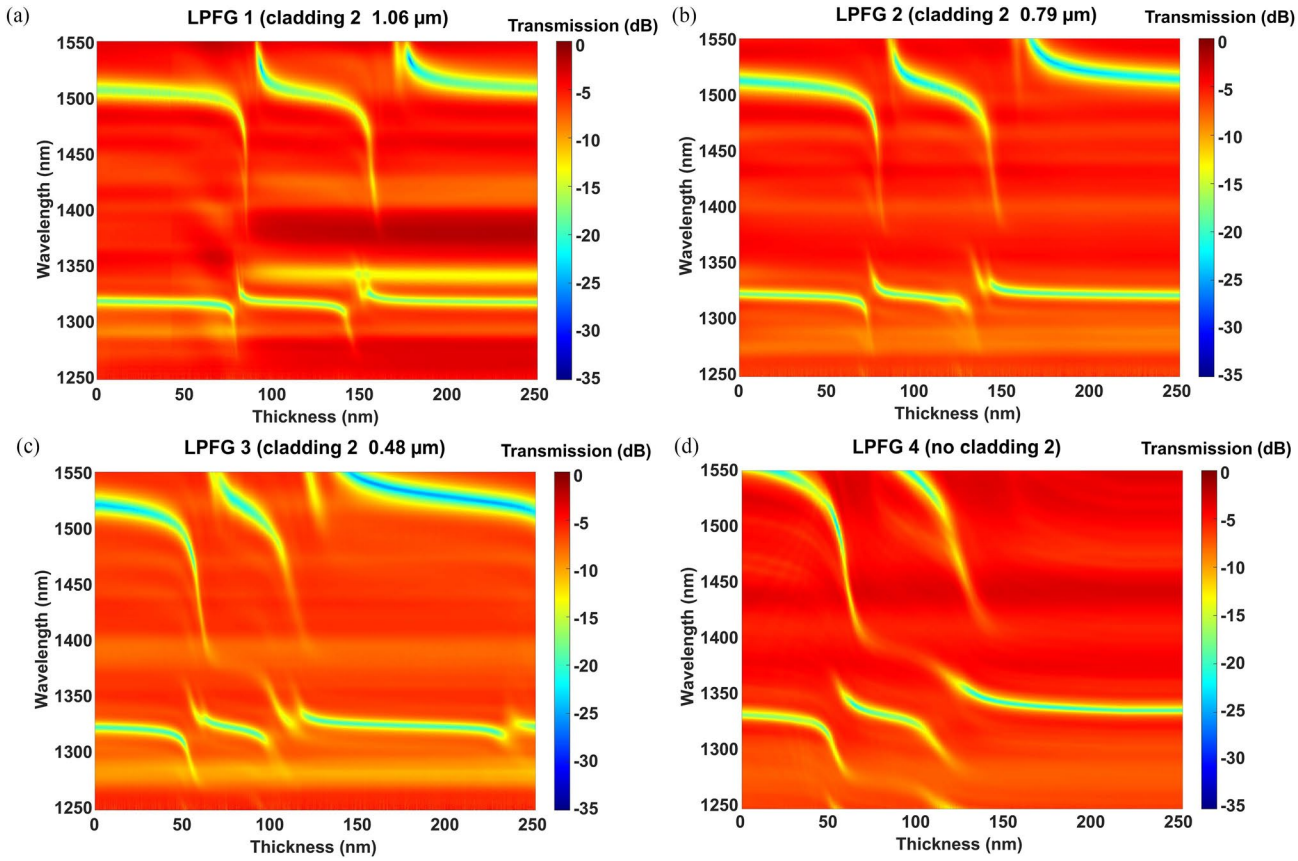

Fig. 7. Experimental results of the wavelength shift in the attenuation bands due to the transitions of the cladding modes with the TiO_2 thin-film thickness. (a) LPFG 1: Cladding 2, 1.06 μm. (b) LPFG 2: Cladding 2, 0.79 μm. (c) LPFG 3: Cladding 2, 0.48 μm. (d) LPFG 4: No Cladding 2, and Cladding 1 etched 0.28 μm.

The results in Fig. 5 show that, when the second-cladding thickness increases, the mode transition generated when one of the cladding modes is guided in the thin film is more abrupt.

This phenomenon has an immediate effect in the evolution of the resonance bands as a function of thickness, given by the phase matching condition [5]:

$$\lambda = (n_{core}(\lambda) - n^{i\ clad}(\lambda))\Lambda \quad (1)$$

where $n_{core}(\lambda)$is the effective index of the core mode at wavelength λ, $n^{i}_{clad}(\lambda)$ is the effective index of the ith cladding mode and Λ is the period of the grating.

In order to verify this assumption, the four LPFGs were deposited with TiO_2 and the transmission spectra registered during the deposition process. Fig. 7 shows the experimental results obtained by using the thicknesses given by the ellipsometer in silicon wafer samples deposited in parallel with the optical fibre. The results in Fig. 7 show the same tendency as that observed in Fig. 5. For a thicker second cladding, the wavelength shifts in the resonances (in yellow) are more abrupt and become progressively smoother from LPG1 to LPG4, i.e., to the case where the second cladding has been completely removed and shows the lowest sensitivity to thickness.

However, it is also important to remark that the increase in sensitivity is not unlimited. In Fig. 7 there is a higher fading and an increase in the full width at half maximum (decrease of the figure of merit) of the resonance bands as the second-cladding thickness increases. This is confirmed in Fig. 8 by showing the spectra in the mode transition region for LPFG 1: the LPFG with a thickest second clad (graphs corresponding to thin film thicknesses between 81 and 88 nm in 0.5 nm intervals are plotted); and for LPFG 4: the LPFG without second clad (thin film thicknesses between 55 and 69 nm in 1 nm intervals, as the shift with thickness is slower).

Fig. 9 shows the numerical (a) and experimental (b) wavelength shift of the $HE_{1,14}$ band, which is the one located initially at around 1500 nm before starting the deposition. The more abrupt wavelength shift for a thicker second cladding is evident. However, the increase in the second-cladding thickness also leads to a fading of the resonance in the transition region in the experiments for two of the cases analyzed: 1.06 μm and 0.79 μm, which is why in a certain region no values are shown for these two cases in Fig. 9(b). In spite of this, it must be highlighted that the calculation of the resonance wavelength with quadratic fitting to a parabola based on a MATLAB routine permits to track the resonance in the 1400–1500 nm wavelength range.

In addition, Fig. 10 shows the theoretical and experimental derivative of the notch wavelength with respect to the film

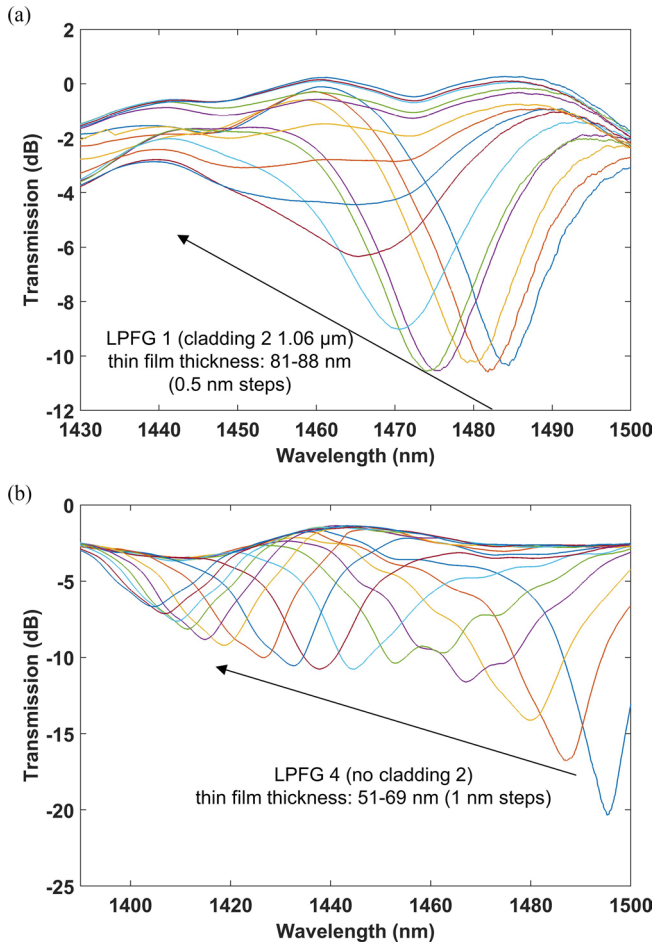

Fig. 8. Transmission spectra in the transition of: (a) LPFG 1 (thickest second clad); (b) LPFG 4 (without second clad).

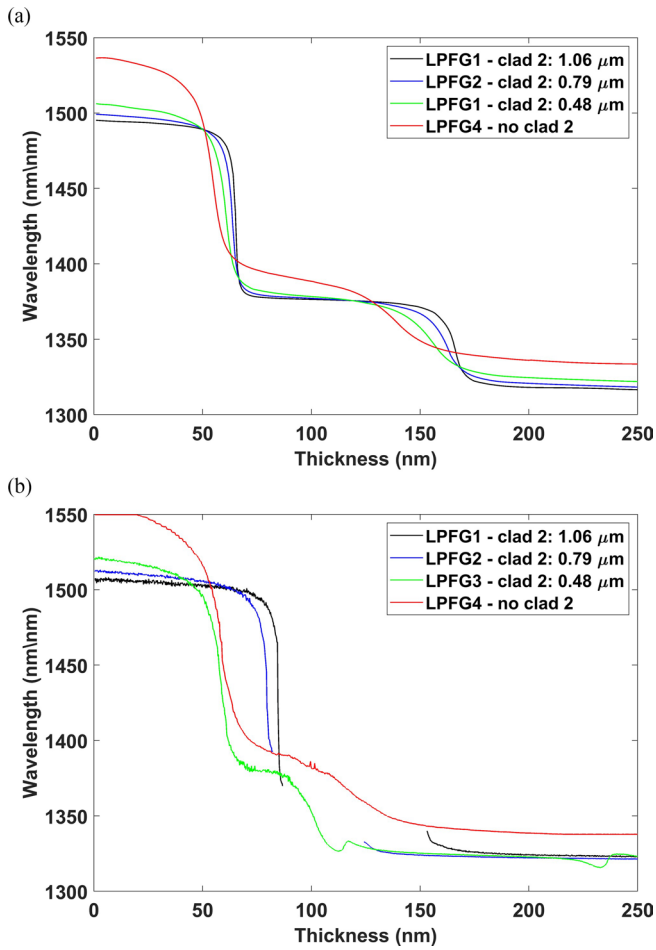

Fig. 9. Wavelength shift of the $HE_{1,14}$ band as a function of thickness. (a) Numerical results. (b) Experimental results. When the second cladding is thicker the $HE_{1,14}$ band fades and it is not possible to extract the wavelength.

thickness for all the fibers analyzed. According to the numerical results, the maximum of the derivative increases and is shifted to a higher thickness when the second cladding is thicker. The experimental results follow the same trend, which demonstrates that the method for estimating the second clad thickness based on the resonance wavelength shift during the etching process is accurate. However, while in the case of the value of the derivative there is a very good agreement between theory and experiment, regarding the thickness there is not such a good fit. This is attributed to the error in the thickness measurement obtained with the ellipsometer and to small difference in the deposition rate of the ALD machine in each experiment. For this last question it must be considered that the reaction chamber was covered with a dome lid (the volume of the chamber is higher than with a flat lid), and the deposited thicknesses are rather big for an ALD.

In order to understand better the enhancement of sensitivity, Fig. 11(a) shows the optical field intensity for LPFG 4 for thicknesses ranging from 55 to 75 nm, where the mode transition takes place. It is evident that the $HE_{1,2}$ mode is guided in the thin film for thicknesses above 65 nm. This agrees with the evolution of the effective index in Fig. 5, where the mode $HE_{1,2}$ increases its effective index abruptly indicating that it is guided in the TiO_2 thin film. The same effect in the field intensity is observed for LPFG 1, with cladding 2, in Fig. 11(b), but with the exception that the guidance of $HE_{1,2}$ mode starts for a thicker thin film. This again agrees with Figs. 5 and 8, where the variations in the effective indices and in the coupling wavelengths occur at greater thicknesses due to the presence of the second cladding between the first cladding and the thin film, acting as a barrier for the guidance of the mode in the thin film.

In addition, Fig 11(c)–(d) shows the radial and azimuthal electric field of the $HE_{1,14}$ mode for LPFG 4 and LPFG 1. It is evident from there, especially at 70nm, that a greater field is detected in the TiO_2 thin film for LPFG 1, which permits relating this enhancement of the field to the sensitivity increase observed in Fig. 7.

C. Refractive Index Sensitivity

In this subsection the capability to control the thickness of the second cladding to optimize the sensitivity to the SRI in the mode transition will be assessed. To this purpose, two different LPFGs were analyzed in order to observe the wavelength shift of the resonance bands. One of these new LPFGs was etched until a wavelength shift of 6 nm was attained (LPFG 5), while the

other was etched until a wavelength shift of 15 nm was achieved (LPFG 6). These wavelength shifts correspond in Fig. 3 to second-cladding thicknesses of 1.13 and 0.61 μm, respectively.

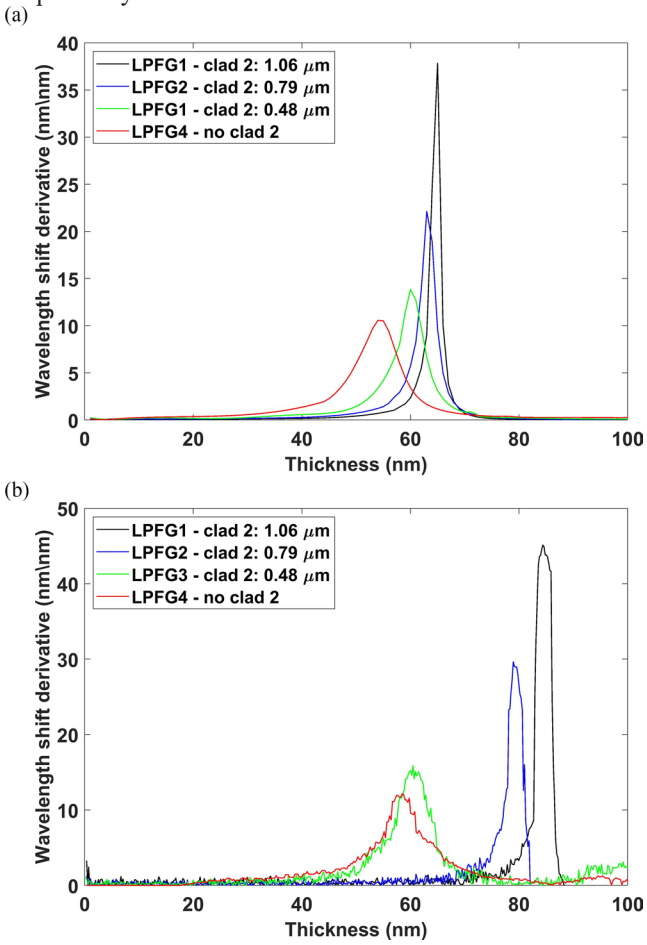

Fig. 10. Derivative of the wavelength shift in the attenuation bands. (a) Numerical results. (b) Experimental results.

After that, both LPFGs were deposited with TiO_2. Before that, some simulations where performed analyzing the mode transition (see Fig. 12). In Fig. 12(a), both cases and the case of no presence of the second clad are presented. As expected, the mode transition is more abrupt for the thicker cladding. It was decided to select a TiO_2 coating thickness of 60 nm as the working point because it is considered that both LPFGs are in the mode transition region for this thickness. This coating thickness corresponds to a wavelength shift of 12.8 nm (LPFG 5, second cladding thickness of 1.13 μm) and 41.4 nm (LPFG 6, second cladding thickness of 0.61 μm), respectively.

In Fig. 12(b), both LPFGs with a TiO_2 coating thickness of 60 nm are analyzed as a function of the surrounding RI, along with an LPFG with no second cladding. The results indicate that a higher sensitivity is obtained by the LPFG with a thicker second cladding, according the analysis of the sensitivity to TiO_2 thickness in Figs. 3 and 4. The region of maximum sensitivity is located at 1.42–1.44, something that is confirmed, along with the improvement in sensitivity with a thicker second cladding, in the experimental results shown in Fig. 13.

In Fig. 13(a) and (b) it is possible to visualize the color map of the experiment, where the resonance bands, with a low transmission, show a yellow color. The first deposition (LPG5, Fig. 13(a)) was stopped after a wavelength shift of 9 nm while the second deposition (LPG 6, Fig. 13(b)) was halted after a wavelength shift of 57 nm, with the aim of generating the mode transition in the same refractive index range (1.42-1.44) for the sake of comparison.

Fig. 13(c) and 13(d) show the results when immersing the LPFGs in liquids of different RI ranging from 1.33 to 1.47 (more details in Methods and Materials), the typical values analyzed when assessing the performance of optical fiber sensors [5]. There it is evident that a much higher sensitivity is achieved with the LPFG with a thicker second cladding (LPFG 5). For instance, with this LPFG sensitivities for the upper wavelength band (in purple) are double in the RI region of 1.435–1.45 compared to the LPFG with thinner cladding. Moreover, values around 5000 nm/RIU are obtained at RI of 1.43–1.44, a result that, except for a publication were a 40000 nm/RIU sensitivity is attained [14], is located on top of the rest of LPFG based publications analyzed in a recent review of optical fiber refractometers, where the best sensitivities are 5000–6000 nm/RIU [5]. In addition, the 5000 nm/RIU value could be improved with an LPFG operating at the dispersion turning point, a case that for the sake of simplicity was not analyzed in this work but that could be explored in a future work. This region of maximum sensitivity agrees well with the simulations in Fig. 13(b).

The higher refractive index sensitivity obtained with LPFG 5, with a thicker second cladding than LPFG 6, follows the same trend observed as a function of the thin film thickness (LPFGs 1–4). This means that a second clad that actuates as an intermediate low refractive index layer between a thin film and the first cladding of the LPFG permits to increase the sensitivity of the optical fiber structure. However, the thickness of the second clad cannot be enlarged without limit because there is an increasing fading of the resonances, something that can be observed in LPFG 5 in Fig. 13(c), where some points in the mode transition are missing due to this reason. The same idea has also been observed in Figs. 7–9 as a function of the nanocoating thickness. There, a higher sensitivity to the thin film thickness and a higher fading is obtained with LPFG 1 and 2, with a thicker second clad than the other two fibers explored, LPFG 3 and 4. One way to mitigate the fading could be to modify the length of the LPFG for a maximum coupling in the mode transition region.

Another important question is tuning the operation point in the case of the refractive index. In Fig. 13, the range with a higher sensitivity is 1.43–1.45 because the deposition was stopped in the middle of the mode transition (thin film thickness of around 60 nm), which permitted to observe a higher wavelength shift and have a better idea of the nanocoating thickness by tracking the resonance. However, depending on the specific refractive index (RI) range in which the maximum sensitivity is desired, a different thin film thickness will be required. All this must be done by considering that the deposition is performed in air (RI = 1), and by calculating with simulations the adequate thickness to attain the best sensitivity in the desired refractive index range. Moreover, the surrounding RI itself may play a role in the sensitivity, that is, for two thin film thicknesses values

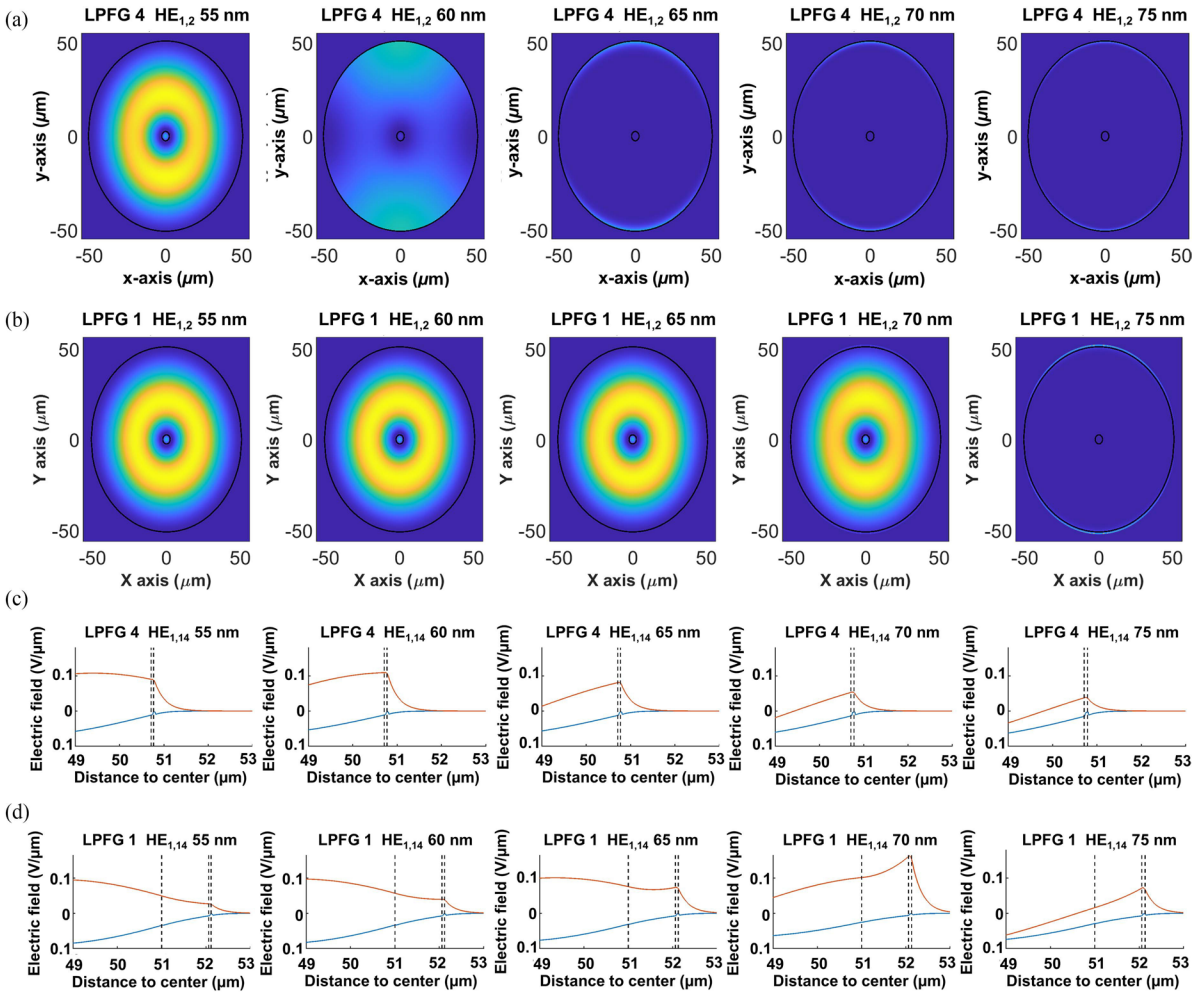

Fig. 11. Calculation of the fields. (a) Field intensity distribution of $HE_{1,2}$ mode in the cross-section of a double-clad fiber as function of the TiO_2 coating thickness for LPFG 4. (b) Same as (a) for LPFG1. (c) Radial (blue) and azimuthal (red) field of $HE_{1,14}$ for LPFG4. (d) Same as (c) for LPFG1.

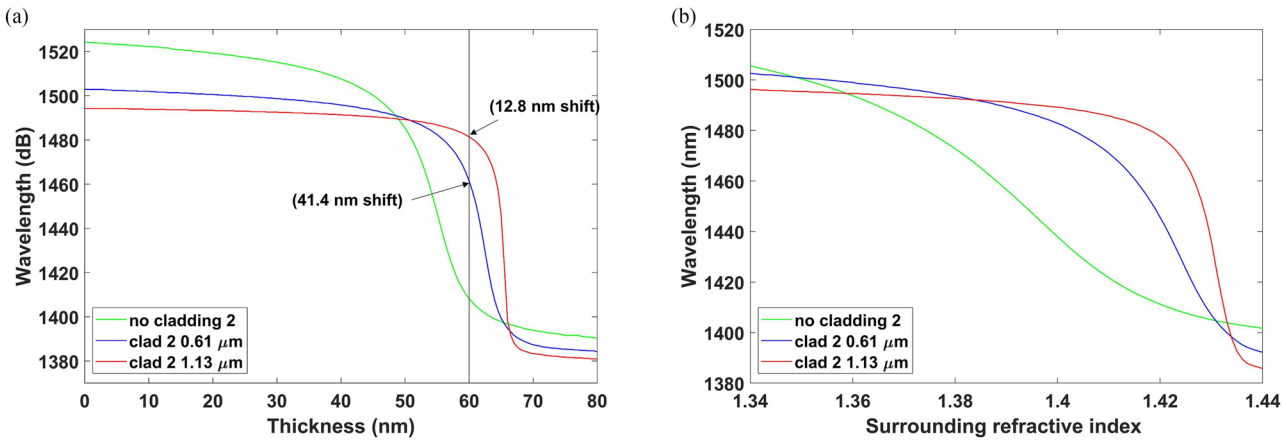

Fig. 12. Numerical analysis of sensitivity to refractive index. (a) Wavelength shift of the $HE_{1,14}$ band as a function of TiO_2 coating thickness for LPFGs without cladding 2 and with cladding 20.61 and 1.13 μm. (b) Wavelength shift of the $HE_{1,14}$ band as a function of the surrounding RI for without cladding 2 and with cladding 20.61 and 1.13 μm.

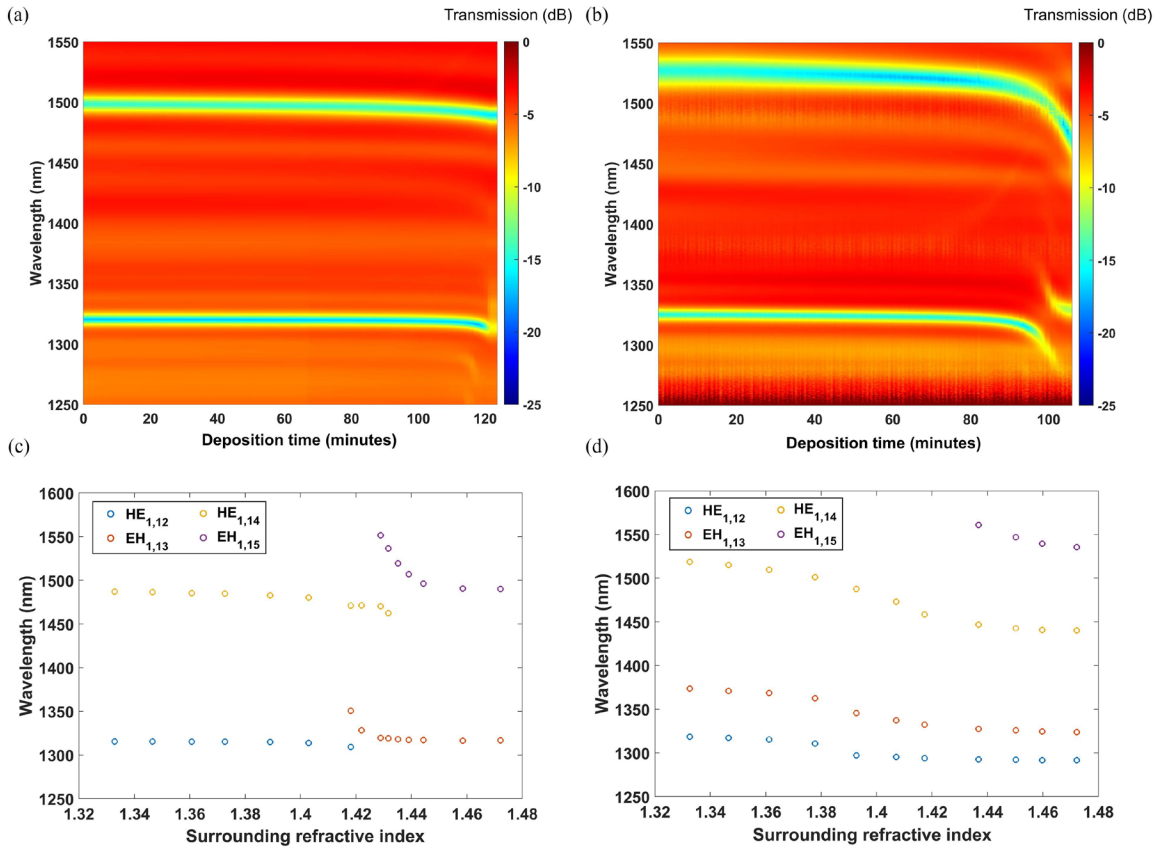

Fig. 13. Sensitivity to refractive index. (a) Transmission spectra of LPFG 5 (cladding thickness 1.13 μm) during the deposition of a TiO_2 thin film, (b) the same for LPFG 6 (cladding thickness 0.61 μm), (c) Characterization as a function of RI of LPFG 5 and (d) Characterization as a function of RI of LPFG 6.

that produce the mode transition in two different RI regions, the maximum sensitivity that can be achieved by increasing the second cladding thickness without fading, might be different. In addition, the results also depend on the refractive index of the nanocoating. Consequently, it is necessary to control several parameters to design sensors with optimum performance in different media, being the easiest one air because the deposition is stopped at the same point the sensor will work in.

IV. Conclusion

The results presented here demonstrate a new way to improve the sensitivity of LPFGs consisting of including an intermediate low-RI layer between the highly refractive thin film responsible for the mode transition and the cladding of the LPFG.

Many years have passed since this idea was first proposed theoretically [16]. This is a result of the great challenge of finding a material with low RI and low absorption, something that can be found in double-clad fibers whose second cladding is doped with fluorine to reduce the RI. Another challenge was to reduce the thickness of the second cladding, which initially was too thick, around 10 μm. Therefore, it was necessary to apply a smooth etching process that permitted achieving a precise control of the second-cladding thickness.

With these two conditions, it was possible with the aid of an ALD process to monitor four different cases where the effect of the intermediate low RI was evident in air, demonstrating that the mode transition phenomenon is tunable with an intermediate low-RI layer.

So far, the mode transition could only be improved by increasing the refractive index of the thin film and by approaching the dispersion turning point. A recent design based on double clad fibers where the second clad presents a higher refractive index (W-type fibers) [22] permits to reduce the fading effect but it is finally the same concept as the single clad fiber with a thin film, that is, a three layer structure where the last layer has a higher refractive index than that of the cladding. Here, with double clad fibers where the second clad presents a low refractive index, a new degree of freedom is offered (its thickness) that can also be applied for improving the performance in liquid surrounding media.

The device with a thicker second cladding showed better sensitivity, with values above 5000 nm/RIU. All this was achieved in a non-optimal device whose period was far from the dispersion turning point. Consequently, there is still room to improve the performance of the proposed devices.

In addition, the required technology can be greatly simplified. Here, an ALD process was used because it permitted observing the very slow evolution of the phenomenon, but other techniques, such as sputtering, could also be employed. Regarding the optical fiber, once an optimal design is obtained, double-clad fibers, where the thickness of the second cladding is initially the

optimal, would permit avoiding the etching process. Although a higher fading was observed when the highest sensitivities were obtained, parameters such as the length of the device or the modulation index could be optimized to reduce this effect. Additionally, the concept of optical fibers with a thin second cladding could be expanded to other structures, such as tilted-fiber Bragg gratings (TFGBs), which suggests that this work could open a new and extensive line of research in the field of optical fiber sensors, expanding and reinforcing their applicability in demanding domains, such as environmental and chemical sensors, biosensors or even the Internet of Things.

References

[1] V. Bhatia and A. M. Vengsarkar, "Optical fiber long-period grating sensors," *Opt. Lett.*, vol. 21, no. 9, pp. 692–694, 1996, doi: 10.1364/ol.21.000692.

[2] A. M. Vengsarkar, J. R. Pedrazzani, J. B. Judkins, P. J. Lemaire, N. S. Bergano, and C. R. Davidson, "Long-period fiber-grating-based gain equalizers," *Opt. Lett.*, vol. 21, no. 5, pp. 336–338, 1996, doi: 10.1364/OL.21.000336.

[3] V. Bhatia, D. Campbell, R. O. Claus, and M. Vengsarkar, "Simultaneous strain and temperature measurement with long-period gratings," *Opt. Lett.*, vol. 22, no. 9, pp. 648–650, 1997, doi: 10.1364/OL.22.000648.

[4] A. B. Socorro-Leránoz, D. Santano, I. Del Villar, and I. R. Matias, "Trends in the design of wavelength-based optical fibre biosensors (2008–2018)," *Biosensors Bioelectron. X*, vol. 1, 2019, Art. no. 100015, doi: 10.1016/j.biosx.2019.100015.

[5] A. Urrutia, I. Del Villar, P. Zubiate, and C. R. Zamarreño, "A comprehensive review of optical fiber refractometers: Toward a standard comparative criterion," *Laser Photon. Rev.*, vol. 13, no. 11, 2019, Art. no. 1900094, doi: 10.1002/lpor.201900094.

[6] X. Shu, X. Zhu, and S. Jiang, "High sensitivity of dual resonant peaks of long-period fibre grating to surrounding refractive index changes," *Electron. Lett.*, vol. 35, no. 18, pp. 1580–1581, 1999.

[7] I. Del Villar, J. L. Cruz, A. B. Socorro, J. M. Corres, F. J. Arregui, and I. R. Matias, "Sensitivity optimization with cladding-etched long period fiber gratings at the dispersion turning point," *Opt. Exp.*, vol. 24, no. 16, pp. 1240–1245, 2016.

[8] I. Del Villar, I. R. Matias, and F. J. Arregui, "Long-period fiber gratings with overlay of variable refractive index," *IEEE Photon. Technol. Lett.*, vol. 17, no. 9, pp. 1893–1895, Sep. 2005.

[9] I. Del Villar, I. Matías, F. Arregui, and P. Lalanne, "Optimization of sensitivity in long period fiber gratings with overlay deposition," *Opt. Exp.*, vol. 13, no. 1, pp. 56–69, 2005.

[10] A. Cusano et al., "Mode transition in high refractive index coated long period gratings," *Opt. Exp.*, vol. 14, no. 1, pp. 19–34, 2006, doi: 10.1364/OPEX.14.000019.

[11] P. Pilla, C. Trono, F. Baldini, F. Chiavaioli, M. Giordano, and A. Cusano, "Giant sensitivity of long period gratings in transition mode near the dispersion turning point : An integrated design approach," *Opt. Lett.*, vol. 37, no. 19, pp. 4152–4154, 2012.

[12] C. S. Cheung, S. M. Topliss, S. W. James, and R. P. Tatam, "Response of fibre optic long period gratings operating near the phase matching turning point to the deposition of nanostructured coatings," *JOSA B*, vol. 25, no. 6, pp. 897–902, 2008, doi: 10.1364/JOSAB.25.000897.

[13] X. Chen, K. Zhou, L. Zhang, and I. Bennion, "Dual-peak long-period fiber gratings with enhanced refractive index sensitivity by finely tailored mode dispersion that uses the light cladding etching technique," *Appl. Opt.*, vol. 46, no. 4, pp. 451–455, 2007, doi: 10.1364/AO.46.000451.

[14] M. S´mietana, M. Koba, P. Mikulic, and W. J. Bock, "Towards refractive index sensitivity of long-period gratings at level of tens of μm per refractive index unit: Fiber cladding etching and nano-coating deposition," *Opt. Exp.*, vol. 24, no. 11, pp. 11897–11904, 2016, doi: 10.1364/OE.24.011897.

[15] P. Zubiate et al., "Fiber-based early diagnosis of venous thromboembolic disease by label-free D-dimer detection," *Biosensors Bioelectron. X*, vol. 2, 2019, Art. no. 100026, doi: 10.1016/j.biosx.2019.100026.

[16] I. Del Villar, I. R. Matias, and F. J. Arregui, "Deposition of coatings on long-period fiber gratings: Tunnel effect analogy," *Opt. Quantum Electron.*, vol. 38, no. 8, pp. 655–665, 2006, doi: 10.1007/s11082-006-9002-3.

[17] N. D. Rees, S. W. James, R. P. Tatam, and G. J. Ashwell, "Optical fiber long-period gratings with Langmuir–Blodgett thin-film overlays," *Opt. Lett.*, vol. 27, no. 9, pp. 686–688, 2002.

[18] I. Del Villar, I. R. Matias, F. J. Arregui, and M. Achaerandio, "Nanodeposition of materials with complex refractive index in long-period fiber gratings," *J. Lightw. Technol.*, vol. 23, no. 12, pp. 4192–4199, 2005, doi: 10.1109/JLT.2005.858246.

[19] A. Cusano et al., "Cladding mode reorganization in high-refractive-index-coated long-period gratings: Effects on the refractive-index sensitivity," *Opt. Lett.*, vol. 30, no. 19, pp. 2536–2538, 2005, doi: 10.1364/OL.30.002536.

[20] F. Zou, Y. Liu, C. Deng, Y. Dong, and S. Zhu, "Refractive index sensitivity of nano-film coated long-period fiber gratings," *Opt. Exp.*, vol. 23, no. 2, pp. 1114–1124, 2015, doi: 10.1364/OE.23.001114.

[21] F. Esposito et al., "Long period grating in double cladding fiber coated with graphene oxide as high-performance optical platform for biosensing," *Biosensors Bioelectron.*, vol. 172, 2021, Art. no. 112747, doi: 10.1016/j.bios.2020.112747.

[22] F. Esposito, A. Srivastava, L. Sansone, M. Giordano, S. Campopiano, and A. Iadicicco, "Sensitivity enhancement in long period gratings by mode transition in uncoated double cladding fibers," *IEEE Sensors J.*, vol. 20, no. 1, pp. 234–241, Jan. 2020, doi: 10.1109/JSEN.2019.2942639.

[23] I. Del Villar, O. Fuentes, F. Chiavaioli, J. M. Corres, and I. R. Matias, "Optimized strain long-period fiber grating (LPFG) sensors operating at the dispersion turning point," *J. Lightw. Technol.*, vol. 36, no. 11, pp. 2240–2247, Jun. 2018, doi: 10.1109/JLT.2018.2790434.

[24] S. W. James and R. P. Tatam, "Optical fibre long-period grating sensors: Characteristics and application," *Meas. Sci. Technol.*, vol. 14, no. 5, pp. R49–R61, 2003, doi: 10.1088/0957-0233/14/5/201.